Journal of
Mechanics of
Materials and Structures

STABILITY AND NONPLANAR POSTBUCKLING BEHAVIOR OF CURRENT-CARRYING MICROWIRES IN A LONGITUDINAL MAGNETIC FIELD

Yuanzhuo Hong, Lin Wang and Hu-Liang Dai

Volume 13, No. 4 July 2018

msp

JOURNAL OF MECHANICS OF MATERIALS AND STRUCTURES
Vol. 13, No. 4, 2018
dx.doi.org/10.2140/jomms.2018.13.481

STABILITY AND NONPLANAR POSTBUCKLING BEHAVIOR OF CURRENT-CARRYING MICROWIRES IN A LONGITUDINAL MAGNETIC FIELD

YUANZHUO HONG, LIN WANG AND HU-LIANG DAI

The stability and nonplanar buckling problem of current-carrying microwires in the presence of longitudinal magnetic field are investigated by accounting for the nonlinearities resulted from the axial elongation of the microwire's centerline. Based on the Euler–Bernoulli beam theory, modified couple stress theory, and Hamilton's principle, the nonlinear governing equations of the nonplanar motions of the microwire are derived. By application of Galerkin's approach, the nonplanar dynamic responses are evaluated for both clamped-clamped and pinned-pinned boundary conditions. The effects of dimensionless material length scale parameter, compressive load, magnetic field force, and slenderness ratio on the nonplanar buckling instability and the postbuckling configuration are discussed in detail. The obtained results show that the nonplanar buckling instability of microwires occurs when the magnetic field force becomes sufficiently large and the postbuckling configuration depends on the magnitude of magnetic field force, slenderness ratio, and initial conditions. The material length scale parameter can stabilize the microwire. Moreover, the stability boundaries for the magnetic field parameter and compressive load are analyzed, showing that an expected critical value of magnetic field parameter may be achieved by choosing a suitable compressive load as a trigger of automatic devices. Interestingly, it is found that the presence of an axial compressive load has no effect on the postbuckling shape, although it can destabilize the microwire system and amplify the postbuckling amplitude.

1. Introduction

With the flourish of nanomaterials and nanotechnology [Lee et al. 2013; Tao et al. 2010; Atashbar and Singamaneni 2005; McFarland and Colton 2005], miniaturization is becoming one of the main features in microelectromechanical systems (MEMS) and microelectronic devices [Lee et al. 2008; Li et al. 2007; Luo et al. 2006; Pauzauskie and Yang 2006; Singh 2009]. For that reason, many scientific researchers have paid great attention to the mechanical behaviors of micro/nano structures. In many practical applications, microstructures may be subjected to various physical fields, such as a magnetic field, electric field, or fluid flow. It has been experimentally observed in the scale of micrometers that strong small-length scale effects may occur in both nonmetallic and metallic materials [McFarland and Colton 2005; Fleck et al. 1994; Stölken and Evans 1998]. Namely, the mechanical properties of microscale structures may depend on their geometrical size. Obviously, such size-dependent properties cannot be classical/conventional continuum mechanics theories. Some experimental results [McFarland and Colton 2005; Fleck et al. 1994; Stölken and Evans 1998] showed that with the decrease of structural

Lin Wang is the corresponding author.

Keywords: nonplanar postbuckling configuration, microwire carrying electric current, modified couple stress theory, longitudinal magnetic field, buckling instability.

characteristic size, the effective stiffness of microscale structures generally becomes higher than that predicted by using the classical continuum mechanics theories, i.e., the error between the experimental result and the result from classical continuum mechanics theories might be remarkable in some cases. Therefore, several nonclassical continuum theories have been established, such as the nonlocal elasticity theory [Wang 2009; Wang et al. 2006; Chang and Yeh 2014], surface elasticity theory [Kiani 2014a; He and Lilley 2008], strain gradient elasticity theory [Ebrahimi and Barati 2017a], and couple stress theory [Yang et al. 2002; Mindlin and Tiersten 1962].

According to the nonlocal elasticity theory, the stress state at a given point is assumed to depend on the strain state of itself and its neighborhood [Wang et al. 2006]. The surface elasticity theory presumes that the surface energy cannot be ignored, and with the increase of ratio between surface/interface area and volume, the effect of surface layer may play a significant role in predicting the mechanical behavior of nanoscale structures [Wang 2009]. The couple stress theory is originally developed by Mindlin and Tiersten [1962] and further modified by Yang et al. [2002]. In the modified couple stress theory, not only the classical normal and shear stresses, but also the couple stresses, which are related to the deformation via a new material constant called the material length scale parameter, have been taken into account. So far, many researchers have utilized the modified couple stress theory to describe the size effect of microstructures [Tsiatas 2009; Dai et al. 2015; Dehrouyeh-Semnani et al. 2015; Mohammadabadi et al. 2015].

In the framework of the above nonclassical continuum theories, there were a few studies focused on the mechanical behavior of carbon nanotubes in magnetic fields [Kiani 2014c; Arani et al. 2015; Wang et al. 2016]. In the presence of a magnetic field, the Lorentz force generated by the induced current needs to be taken into account in some cases. For instance, Kiani [2014c] investigated the instability of a single-walled carbon nanotube (SWCNT) subjected to a three-dimensional (3D) magnetic field and obtained the critical transverse magnetic field at which buckling instability of the SWCNT occurs. Arani et al. [2015] studied the nonlinear vibration of two coupled nanotubes conveying fluid under a two-dimensional (2D) magnetic field, showing that the effect of a transverse magnetic field on the stability of CNTs is more obvious than that of a longitudinal magnetic field. More recently, Wang et al. [2016] studied the natural frequency and stability of fluid-conveying carbon nanotubes in a longitudinal magnetic field, and they found that the magnetic field can increase the critical flow velocity for flutter instability.

In addition, there were some studies associated with the vibration characteristics of micro/nano-beams acted upon by magnetic fields [Chang 2016; Ebrahimi and Barati 2016; 2017b]. For instance, Chang [2016] analyzed the effect of a magnetic field on the frequency of nonlinear nanobeams based on nonlocal elasticity theory and found that the magnetic force decreases the frequency and hence the nonlocal parameter can destabilize the nanobeam. Ebrahimi and Barati [2016] established a dynamical model of thermo-piezo-electrically actuated nanobeams under a magnetic field. On the basis of nonlocal strain gradient theory, Ebrahimi and Barati [2017b] investigated the flexural wave propagation of functionally graded (FG) nanobeams in a longitudinal magnetic field. It was shown that the wave propagation characteristics of FG nanobeams depend on various parameters including material graduation, magnetic field intensity, and length scale parameter.

In the past years, several investigations have been carried out regarding the dynamics of micro/nano-wires carrying electric current in the presence of magnetic fields [Kiani 2014a; 2015a; Wang et al. 2015]. In the dynamical model of current-carrying micro/nano-wires under magnetic fields, the induced current for the change of magnetic flux was assumed to be negligible if compared with the initial current. Hence,

the Lorentz force produced by the exerted magnetic field and initial current is the key factor needed to be accounted for.

Reviewing the studies on instability and vibration of magnetically affected micro/nano-wires carrying electric current, Kiani [2014a] studied the forced vibration of current-carrying nanowires (CCNW) in a longitudinal magnetic field accounting for both surface energy and nonlocal size effects. The influence of excitation frequency, magnetic force and small scale parameter on the maximum magnitude of transverse displacements of the CCNW was discussed. Using surface elasticity theory and considering the effect of longitudinal magnetic field, Keivan also investigated the column buckling of doubly parallel slender CCNW [Kiani 2016], and the free vibration and instability of a single CCNW modeled by a string [Kiani 2014b] or by an Euler–Bernoulli beam [Kiani 2015a]. The work of Kiani [2015b] was concerned with the vibration and buckling instability of pretensioned CCNWs acted upon by a suddenly applied 3D magnetic field. Using the differential quadrature method, Wang et al. [2015] calculated the natural frequency and buckling shapes of current-carrying microwires (CCMW) immersed in a longitudinal magnetic field. It was shown that both first- and second-mode buckling instabilities of microwires with clamped-clamped ends might occur when the magnetic field parameter becomes sufficiently large.

Amongst the valuable studies reviewed above, most researchers employed linear analytical models to analyze the dynamical system of magnetically affected CCNWs/CCMWs. However, some key questions associated with nonlinear phenomena cannot be answered excepted by nonlinear theory. For example, when a magnetically affected CCMW is buckled, the original straight equilibrium has become unstable and any motions actually would take place about the new nontrivial equilibrium points. In such a case, the postbuckling behavior must be assessed in the framework of nonlinear theories. Therefore, it is instructive for us to develop nonlinear analytical models for investigating the nonlinear postbuckling behaviors of CCMWs/CCNWs acted upon by magnetic fields.

In the present study, using the modified couple stress theory proposed by Yang et al. [2002], a nonlinear analytical model for magnetically affected CCMWs is developed to explore the microwire's dynamical behavior. Using Hamilton's principle, the nonplanar governing equations are derived by significantly accounting for the nonlinearity associated with the axial extension of the microwire when lateral displacements occur. The main feature of this analytical model is that it is capable of predicting the nonplanar configuration of the CCMW during buckling. The partial differential equations were discretized by Galerkin's approach and the resultant ordinary differential equations (ODE) were further solved via a fourth-order Runge–Kutta method. The effects of slenderness ratio, magnetic field force, axial compressive load, material length scale parameter, and initial conditions on the instability and nonplanar postbuckling configurations are evaluated, interestingly showing that the postbuckling shape of CCMWs is sensitive to the magnetic field parameter as well as the initial conditions employed.

2. Definition, assumption, and modeling of the problem

Consider a straight elastic microwire of length L illustrated in Figure 1. The microwire is immersed in a longitudinal magnetic field $\boldsymbol{B}$ and a constant electric current $\boldsymbol{I}$ is flowing through it. It is assumed that the microwire is slender enough such that the microwire can be modeled by a Euler–Bernoulli microbeam of density ρ, circular cross-sectional area A, and classical flexural rigidity EI. The effects of gravity are neglected while the axial extension of the microwire's centerline is taken into account. The initial

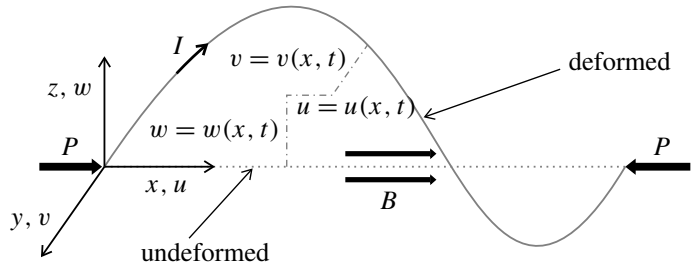

Figure 1. Schematic of a current-carrying microwire in a longitudinal magnetic field.

stress of the microwire may be nonzero due to the action of a given axial compressive load P. In the following analysis, using the rectangular Cartesian coordinate system (x, y, z) shown in Figure 1, the x-axis is assumed to be coincident with the centroidal axis of the undeformed microwire. The microwire may deflect along the y-axis and the z-axis, as shown in Figure 1.

According to the modified couple stress theory [Yang et al. 2002], the relation between the deviatoric part of the coupled stress tensor m_{ij} and the symmetric curvature tensor x_{ij} is given by

$$m_{ij} = 2l^2 G x_{ij}, \tag{1}$$

where G and l represent the shear modulus and the material length scale parameter respectively. By referring to the derivation of Mojahedi and Rahaeifard [2016], the nonzero components of the symmetric curvature tensor can be written as

$$x_{xy} = x_{yx} = -\frac{1}{2}\frac{\partial^2 w}{\partial x^2}, \quad x_{xz} = x_{zx} = -\frac{1}{2}\frac{\partial^2 v}{\partial x^2}. \tag{2}$$

Substituting (2) into (1), one has

$$m_{xy} = m_{yx} = -Gl^2\frac{\partial^2 w}{\partial x^2}, \quad m_{xz} = m_{zx} = -Gl^2\frac{\partial^2 v}{\partial x^2}. \tag{3}$$

As shown in Figure 1, the components of the displacement vector of the point $(x, 0, 0)$ on the centroidal axis can be described as $u = u(x, t)$, $v = v(x, t)$, and $w = w(x, t)$. According to the Euler–Bernoulli beam theory, the displacement field can be written as

$$u_1(x, y, z, t) = u(x, t) - z\frac{\partial w(x, t)}{\partial x} - y\frac{\partial v(x, t)}{\partial x}, \quad u_2 = v(x, t), \quad u_3 = w(x, t), \tag{4}$$

where u_1, u_2, and u_3 are, respectively, the x-, y-, and z-components of the displacement vector $\boldsymbol{u}$ of a point (x, y, z) on a beam cross-section.

The initial axial strain induced by the axial compressive load can be written as

$$\varepsilon_0 = -\frac{P}{EA}. \tag{5}$$

The axial strain caused by the beam's deformation can be obtained by the von-Kármán relation and is given by

$$\varepsilon_1 = \frac{\partial u_1}{\partial x} + \frac{1}{2}\left(\frac{\partial w}{\partial x}\right)^2 + \frac{1}{2}\left(\frac{\partial v}{\partial x}\right)^2 = \frac{\partial u}{\partial x} - z\frac{\partial^2 w}{\partial x^2} - y\frac{\partial^2 v}{\partial x^2} + \frac{1}{2}\left(\frac{\partial w}{\partial x}\right)^2 + \frac{1}{2}\left(\frac{\partial v}{\partial x}\right)^2. \tag{6}$$

It is assumed that the effect of motions on the initial axial strain could be neglected for small deformations. Thus, the total axial strain of the microwire is obtained as

$$\varepsilon_x = -\frac{P}{EA} + \frac{\partial u}{\partial x} - z\frac{\partial^2 w}{\partial x^2} - y\frac{\partial^2 v}{\partial x^2} + \frac{1}{2}\left(\frac{\partial w}{\partial x}\right)^2 + \frac{1}{2}\left(\frac{\partial v}{\partial x}\right)^2, \tag{7}$$

and the axial stress can be written as

$$\sigma_x = E\left[-\frac{P}{EA} + \frac{\partial u}{\partial x} - z\frac{\partial^2 w}{\partial x^2} - y\frac{\partial^2 v}{\partial x^2} + \frac{1}{2}\left(\frac{\partial w}{\partial x}\right)^2 + \frac{1}{2}\left(\frac{\partial v}{\partial x}\right)^2\right]. \tag{8}$$

Now the total strain energy in the microwire can be expressed as

$$V = \frac{1}{2}\int_L \iint_A (\sigma_x \varepsilon_x + m_{xy}x_{xy} + m_{yx}x_{yx} + m_{xz}x_{xz} + m_{zx}x_{zx})\,\mathrm{d}A\,\mathrm{d}x. \tag{9}$$

Substituting (2), (3), (7), and (8) into (9), one obtains

$$V = \frac{1}{2}\int_L \iint_A \left\{E\left[-\frac{P}{EA} + \frac{\partial u}{\partial x} - z\frac{\partial^2 w}{\partial x^2} - y\frac{\partial^2 v}{\partial x^2} + \frac{1}{2}\left(\frac{\partial w}{\partial x}\right)^2 + \frac{1}{2}\left(\frac{\partial v}{\partial x}\right)^2\right]^2 + Gl^2\left(\frac{\partial^2 w}{\partial x^2}\right)^2 + Gl^2\left(\frac{\partial^2 v}{\partial x^2}\right)^2\right\}\mathrm{d}A\,\mathrm{d}x. \tag{10}$$

The kinetic energy of the microwire is given by

$$T = \tfrac{1}{2}\rho A\int_0^L \left[\left(\frac{\partial u}{\partial t}\right)^2 + \left(\frac{\partial v}{\partial t}\right)^2 + \left(\frac{\partial w}{\partial t}\right)^2\right]\mathrm{d}x, \tag{11}$$

where the components of the velocity vector of the point $(x, 0, 0)$ on the centroidal axis are utilized to determine the kinetic energy of the system.

On the basis of Lorentz's formula, the CCMW immersed in a magnetic field would be subjected to a Lorentz force. For small deformations, $\boldsymbol{I} = I_0(1+\partial u/\partial x)\,\boldsymbol{e}_x + I_0(\partial w/\partial x)\,\boldsymbol{e}_y + I_0(\partial v/\partial x)\,\boldsymbol{e}_z$ is the electric current vector with amplitude I_0. According to the derivation of He and Lilley [2008], the Lorentz force per unit length of the microwire immersed in a longitudinal magnetic field can be evaluated by

$$\boldsymbol{f_m} = \boldsymbol{I} \times \boldsymbol{B} = B_0 I_0\left(0\,\boldsymbol{e}_x, \frac{\partial w}{\partial x}\,\boldsymbol{e}_y, -\frac{\partial v}{\partial x}\,\boldsymbol{e}_z\right), \tag{12}$$

where $\boldsymbol{e}_x$, $\boldsymbol{e}_y$, and $\boldsymbol{e}_z$ represent the unit vectors associated with x-, y-, and z-axes, respectively; B_0 is the magnitude of the magnetic induction vector $\boldsymbol{B}$. It is noted that an induced current may be generated because of the electromagnetic induction, yielding an additional magnetic force. According to derivation of Narendar et al. [2012], one obtains the additional magnetic forces along the z- and y-axes are $\eta A H_x^2\,\partial^2 w/\partial x^2$ and $\eta A H_x^2\,\partial^2 v/\partial x^2$, respectively, where η is the magnetic field permeability and H_x is the magnetic flux vector with amplitude H_x in the x direction. In this paper, the microwire is considered to be nonferromagnetic. For nonferromagnetic materials (e.g., copper or silver), the magnetic field permeability η is approximately to be $4\pi \times 10^{-7}$ H/m and the magnetic field intensity $\boldsymbol{H}_x$ is approximately equal to the magnetic induction $\boldsymbol{B}$. In this case, the Lorentz force plays a major role. Thus the effect of the additional magnetic force will be neglected in this work.

Then, the variation of the virtual work resulted from the Lorentz's force is given by

$$\delta W = BI_0 \int_0^L \left(\frac{\partial w}{\partial x} \delta v - \frac{\partial v}{\partial x} \delta w \right) \mathrm{d}x. \tag{13}$$

According to Hamilton's principle, one has

$$\int_{t_1}^{t_2} (\delta V - \delta T - \delta W)\, \mathrm{d}t = 0. \tag{14}$$

Substituting (10), (11), and (13) into (14) and considering the pinned-pinned or clamped-clamped boundary conditions of the microwire, the nonplanar version of the governing equations of the microwire carrying current in a longitudinal magnetic field takes the form

$$\rho A \frac{\partial^2 u}{\partial t^2} - EA \frac{\partial^2 u}{\partial x^2} - EA \frac{\partial v}{\partial x} \frac{\partial^2 v}{\partial x^2} - EA \frac{\partial w}{\partial x} \frac{\partial^2 w}{\partial x^2} = 0, \tag{15a}$$

$$\rho A \frac{\partial^2 v}{\partial t^2} + (AGl^2 + EI) \frac{\partial^4 v}{\partial x^4} + EA \left[\frac{P}{EA} - \frac{\partial u}{\partial x} - \frac{1}{2} \left(\frac{\partial w}{\partial x} \right)^2 - \frac{3}{2} \left(\frac{\partial v}{\partial x} \right)^2 \right] \frac{\partial^2 v}{\partial x^2} - EA \left(\frac{\partial^2 u}{\partial x^2} + \frac{\partial w}{\partial x} \frac{\partial^2 w}{\partial x^2} \right) \frac{\partial v}{\partial x} = BI_0 \frac{\partial w}{\partial x}, \tag{15b}$$

$$\rho A \frac{\partial^2 w}{\partial t^2} + (AGl^2 + EI) \frac{\partial^4 w}{\partial x^4} + EA \left[\frac{P}{EA} - \frac{\partial u}{\partial x} - \frac{1}{2} \left(\frac{\partial v}{\partial x} \right)^2 - \frac{3}{2} \left(\frac{\partial w}{\partial x} \right)^2 \right] \frac{\partial^2 w}{\partial x^2} - EA \left(\frac{\partial^2 u}{\partial x^2} + \frac{\partial v}{\partial x} \frac{\partial^2 v}{\partial x^2} \right) \frac{\partial w}{\partial x} = -BI_0 \frac{\partial v}{\partial x}. \tag{15c}$$

From (15), it is seen that the distributed Lorentz force is not constant but actually depends upon the deformed configuration of the microwire. When we consider the interaction between the magnetic field and microwire, it is also assumed that there is no coupling at the material level but only through the Lorentz force, which is applied as a body force in (15b) and (15c).

In consideration of no distributed axial load, the longitudinal inertia could be neglected [Kahrobaiyan et al. 2011] and (15a) can be reduced to the following form

$$-EA \frac{\partial^2 u}{\partial x^2} - EA \frac{\partial v}{\partial x} \frac{\partial^2 v}{\partial x^2} - EA \frac{\partial w}{\partial x} \frac{\partial^2 w}{\partial x^2} = 0, \tag{16}$$

namely,

$$-\frac{\partial^2 u}{\partial x^2} = \frac{1}{2} \left\{ \frac{\partial}{\partial x} \left[\left(\frac{\partial v}{\partial x} \right)^2 + \left(\frac{\partial w}{\partial x} \right)^2 \right] \right\}. \tag{17}$$

Carrying out two integrations of (17) and applying the corresponding boundary conditions, one obtains

$$u = -\frac{1}{2} \int_0^x \left[\left(\frac{\partial v}{\partial x} \right)^2 + \left(\frac{\partial w}{\partial x} \right)^2 \right] \mathrm{d}x + \frac{x}{2L} \int_0^L \left[\left(\frac{\partial v}{\partial x} \right)^2 + \left(\frac{\partial w}{\partial x} \right)^2 \right] \mathrm{d}x. \tag{18}$$

Substituting (18) into (15b) and (15c), the governing equations of the microwire can be simplified to two-dimensional forms, as follows:

$$(AGl^2+EI)\frac{\partial^4 v}{\partial x^4}+EA\Big[\frac{P}{EA}-\frac{C}{2L}\Big]\frac{\partial^2 v}{\partial x^2}+\rho A\frac{\partial^2 v}{\partial t^2}=BI_0\frac{\partial w}{\partial x}, \tag{19a}$$

$$(AGl^2+EI)\frac{\partial^4 w}{\partial x^4}+EA\Big[\frac{P}{EA}-\frac{C}{2L}\Big]\frac{\partial^2 w}{\partial x^2}+\rho A\frac{\partial^2 w}{\partial t^2}=-BI_0\frac{\partial v}{\partial x}, \tag{19b}$$

where the parameter C represents the axial elongation of the centroidal axis and is defined by

$$C=\int_0^L\Big[\Big(\frac{\partial v}{\partial x}\Big)^2+\Big(\frac{\partial w}{\partial x}\Big)^2\Big]\,\mathrm{d}x. \tag{20}$$

The resultant equations may be rendered dimensionless through the use of

$$\xi=\frac{x}{L},\quad \bar v=\frac{v}{L},\quad \bar w=\frac{w}{L},\quad \tau=\Big[\frac{EI}{\rho A}\Big]^{1/2}\frac{t}{L^2}. \tag{21}$$

The dimensionless equations are

$$(\mu+1)\frac{\partial^4\bar v}{\partial\xi^4}+(p-\alpha c)\frac{\partial^2\bar v}{\partial\xi^2}-\alpha^{3/2}f_I\frac{\partial\bar w}{\partial\xi}+\frac{\partial^2\bar v}{\partial\tau^2}=0, \tag{22a}$$

$$(\mu+1)\frac{\partial^4\bar w}{\partial\xi^4}+(p-\alpha c)\frac{\partial^2\bar w}{\partial\xi^2}+\alpha^{3/2}f_I\frac{\partial\bar v}{\partial\xi}+\frac{\partial^2\bar w}{\partial\tau^2}=0, \tag{22b}$$

where several other dimensionless parameters are defined by

$$\mu=\frac{AGl^2}{EI},\quad p=\frac{PL^2}{EI},\quad f_I=\frac{2\sqrt{2}\,BI_0}{E\pi D},\quad \alpha=\frac{AL^2}{2I}=8\Big(\frac{L}{D}\Big)^2,\quad c=\int_0^1\Big[\Big(\frac{\partial\bar v}{\partial\xi}\Big)^2+\Big(\frac{\partial\bar w}{\partial\xi}\Big)^2\Big]\,\mathrm{d}\xi. \tag{23}$$

The various dimensionless parameters in (23) denote, respectively, the dimensionless material length scale parameter, dimensionless compressive load, dimensionless magnetic force, dimensionless parameter associated with slenderness ratio, and dimensionless axial elongation of the centerline. In the following analysis, the effects of the first four dimensionless parameters appearing in (23) on the stability and nonplanar buckling of the microwire will be discussed in detail.

In the case of a clamped-clamped microwire carrying current, the dimensionless boundary conditions to be satisfied are as follows:

$$\bar v(0,\tau)=\bar v(1,\tau)=0,\qquad \frac{\partial\bar v(0,\tau)}{\partial\xi}=\frac{\partial\bar v(1,\tau)}{\partial\xi}=0, \tag{24a}$$

$$\bar w(0,\tau)=\bar w(1,\tau)=0,\qquad \frac{\partial\bar w(0,\tau)}{\partial\xi}=\frac{\partial\bar w(1,\tau)}{\partial\xi}=0. \tag{24b}$$

The dimensionless boundary conditions for a pinned-pinned microwire may be written in a similar way:

$$\bar{v}(0,\tau)=\bar{v}(1,\tau)=0,\qquad \frac{\partial^2\bar{v}(0,\tau)}{\partial\xi^2}=\frac{\partial^2\bar{v}(1,\tau)}{\partial\xi^2}=0, \tag{25a}$$

$$\bar{w}(0,\tau)=\bar{w}(1,\tau)=0,\qquad \frac{\partial^2\bar{w}(0,\tau)}{\partial\xi^2}=\frac{\partial^2\bar{w}(1,\tau)}{\partial\xi^2}=0. \tag{25b}$$

3. Solutions based on Galerkin's approach

In this section, the Galerkin's approach is applied to transform the governing equations from partial differential equations (PDEs) to ordinary differential equations (ODEs). The resultant ODEs will be further solved by using a fourth-order Runge–Kutta (R–K) method. For the sake of eliminating the effects of initial conditions on the transient responses and achieving steady buckling deformation of the microwire, an additional damping term is added to the governing equations; thus, we have

$$(\mu+1)\frac{\partial^4\bar{v}}{\partial\xi^4}+(p-\alpha c)\frac{\partial^2\bar{v}}{\partial\xi^2}-\alpha^{3/2}f_I\frac{\partial\bar{w}}{\partial\xi}+\frac{\partial^2\bar{v}}{\partial\tau^2}+\gamma\frac{\partial\bar{v}}{\partial\tau}=0, \tag{26a}$$

$$(\mu+1)\frac{\partial^4\bar{w}}{\partial\xi^4}+(p-\alpha c)\frac{\partial^2\bar{w}}{\partial\xi^2}+\alpha^{3/2}f_I\frac{\partial\bar{v}}{\partial\xi}+\frac{\partial^2\bar{w}}{\partial\tau^2}+\gamma\frac{\partial\bar{w}}{\partial\tau}=0, \tag{26b}$$

where γ is a dimensionless damping coefficient. It should be explained that the additional damping term cannot affect the postbuckling configuration of the current-carrying microwire. In what follows, the damping coefficient of $\gamma=1$ is adopted for the purpose of obtaining fast convergence speed.

According to the Galerkin's approach, the dimensionless lateral displacements of the microwire may be expressed as

$$\bar{v}(\xi,\tau)=\sum_{n=1}^{N}\phi_n(\xi)\,q_{vn}(\tau), \tag{27a}$$

$$\bar{w}(\xi,\tau)=\sum_{n=1}^{N}\phi_n(\xi)\,q_{wn}(\tau), \tag{27b}$$

where N is the number of considered modes and $\phi_n(\xi)$ is the n-th mode function of an Euler–Bernoulli beam with corresponding boundary conditions; $q_{vn}(\tau)$ and $q_{wn}(\tau)$ are the two generalized coordinates of the discretized system. It is presumed that the approximate expansion of series (27) may be reliable at a suitably high value of N.

Substituting (27a) and (27b) into (26a) and (26b), one obtains the following set of nonlinear algebraic equations:

$$\begin{bmatrix}\boldsymbol{K}^{vv}(\tau) & \boldsymbol{K}^{vw}\\ \boldsymbol{K}^{wv} & \boldsymbol{K}^{ww}(\tau)\end{bmatrix}\begin{Bmatrix}\boldsymbol{q}_v\\ \boldsymbol{q}_w\end{Bmatrix}+\begin{Bmatrix}\ddot{\boldsymbol{q}}_v\\ \ddot{\boldsymbol{q}}_w\end{Bmatrix}+\gamma\begin{Bmatrix}\dot{\boldsymbol{q}}_v\\ \dot{\boldsymbol{q}}_w\end{Bmatrix}=0, \tag{28}$$

where single and double dots denote first- and second-order derivatives with respect to the dimensionless

time τ. In (28), several vectors and matrices are defined by

$$\boldsymbol{q}_v = \begin{Bmatrix} q_{v1}(\tau) \\ \vdots \\ q_{vN}(\tau) \end{Bmatrix}, \quad \boldsymbol{q}_w = \begin{Bmatrix} q_{w1}(\tau) \\ \vdots \\ q_{wN}(\tau) \end{Bmatrix}, \tag{29a}$$

$$\boldsymbol{K}_{mn}^{vv}(\tau) = \boldsymbol{K}_{mn}^{ww}(\tau) = (\mu+1)\lambda_m^4\delta_{mn} + \eta(\tau)\,\boldsymbol{c}_{mn}, \tag{29b}$$

$$\boldsymbol{K}_{mn}^{vw} = -f_I\boldsymbol{b}_{mn}, \tag{29c}$$

$$\boldsymbol{K}_{mn}^{wv} = f_I\boldsymbol{b}_{mn}. \tag{29d}$$

The values of $\boldsymbol{b}_{mn}$, $\boldsymbol{c}_{mn}$, and λ_n, which are related to the boundary conditions of the microwire, may be evaluated in closed form by defining the following set of constants:

$$\boldsymbol{b}_{mn} = \int_0^1 \phi_m(\xi)\,\phi_n'(\xi)\,\mathrm{d}\xi, \quad \boldsymbol{c}_{mn} = \int_0^1 \phi_m(\xi)\,\phi_n''(\xi)\,\mathrm{d}\xi. \tag{30}$$

For clamped-clamped boundary conditions, we have

$$\lambda_1 = 4.7300, \quad \lambda_2 = 7.8532, \quad \lambda_n \approx \left(n+\tfrac{1}{2}\right)\pi \quad (n = 3, 4, 5, \ldots), \tag{31a}$$

$$\phi_n(\xi) = \cos(\lambda_n\xi) - \cosh(\lambda_n\xi) - \frac{\cos(\lambda) - \cosh(\lambda_n)}{\sin(\lambda_n) - \sinh(\lambda_n)}[\sin(\lambda_n\xi) - \sinh(\lambda_n\xi)]. \tag{31b}$$

For pinned-pinned boundary conditions, one has

$$\lambda_n = n\pi \quad (n = 1, 2, 3, \ldots), \tag{32a}$$

$$\phi_n(\xi) = \sqrt{2}\,\sin(\lambda_n\xi). \tag{32b}$$

It should be noted that the dimensionless parameter $\eta(\tau)$ in (29b) represents the equivalent axial compression p determined by the initial axial compression and the time-varying axial elongation $c(\tau)$, i.e.,

$$\eta(\tau) = p - ac(\tau), \tag{33}$$

$$c(\tau) = \int_0^1 \left\{ \left[\sum_{n=1}^{N} \phi_n'(\xi)\,q_{vn}(\tau) \right]^2 + \left[\sum_{n=1}^{N} \phi_n'(\xi)\,q_{wn}(\tau) \right]^2 \right\} \mathrm{d}\xi. \tag{34}$$

In order to apply the Runge–Kutta method, we define two new vectors as follows

$$\boldsymbol{q} = \begin{Bmatrix} \boldsymbol{q}_v \\ \boldsymbol{q}_w \end{Bmatrix}, \quad \boldsymbol{Q} = \begin{Bmatrix} \dot{\boldsymbol{q}} \\ \boldsymbol{q} \end{Bmatrix}. \tag{35}$$

Then one obtains

$$\dot{\boldsymbol{Q}} = F(\tau, \boldsymbol{Q}) = \begin{bmatrix} -\gamma \times [\boldsymbol{I}] & -[\boldsymbol{K}] \\ [\boldsymbol{I}] & [\boldsymbol{0}] \end{bmatrix} \begin{Bmatrix} \{\dot{\boldsymbol{q}}\} \\ \{\dot{\boldsymbol{q}}\} \end{Bmatrix}, \tag{36}$$

where $[\boldsymbol{I}]$ is a unit diagonal matrix and $[\boldsymbol{0}]$ is a zero element matrix.

By use of the fourth-order Runge–Kutta method, the dynamic responses of the CCMW immersed in a longitudinal magnetic field may be calculated. Selecting a set of system parameters defined in (23), one

can analyze the effects of slenderness ratio, magnetic force, axial compression and material length scale parameter on the stability and nonplanar postbuckling behaviors of the microwire.

4. Validity of the developed nonlinear model and proposed computational procedure

It is noted that, due to the presence of Lorentz's force, (26) could not be solved analytically. In the case of $f_I = 0$, however, the exact solutions for the postbuckling amplitudes of a microwire under axial compression are available [Nayfeh and Emam 2008]. In this section, first, numerical simulations based on (26) are performed in order to check the validity of the developed nonlinear model and proposed computational procedure. For that purpose, the postbuckling configuration of an axially loaded microbeam in the absence of magnetic fields is numerically calculated and compared to that obtained analytically.

In the case of $\mu = 0$ and $f_I = 0$, (26) is reduced to the buckling problem of a classical Euler–Bernoulli beam subjected to a compressive load. The governing equation for the planar deflection of the microwire becomes

$$\psi^{iv}(\xi) + p\psi''(\xi) - \alpha\psi'' \int_0^1 \psi'^2(\xi)\,\mathrm{d}\xi = 0. \tag{37a}$$

Now consider a simply-supported beam with an axial compressive load of $p = 10\pi^2$. In this case, the analytical solution for the buckling configuration is given by [Sun et al. 2017]

$$\psi_1(\xi) = \pm\frac{3\sqrt{2\alpha}}{\alpha}\sin(\pi\xi). \tag{37b}$$

As seen in Figure 2, compared with the analytical solution of (37b), our numerical results for the buckling amplitude of the microwire achieve low relative error below 0.01% for $N > 4$, thus demonstrating the validation and accuracy of the Runge–Kutta procedure. Synthesizing both the accuracy and computational efficiency, therefore, $N = 5$ will be chosen for the following calculations.

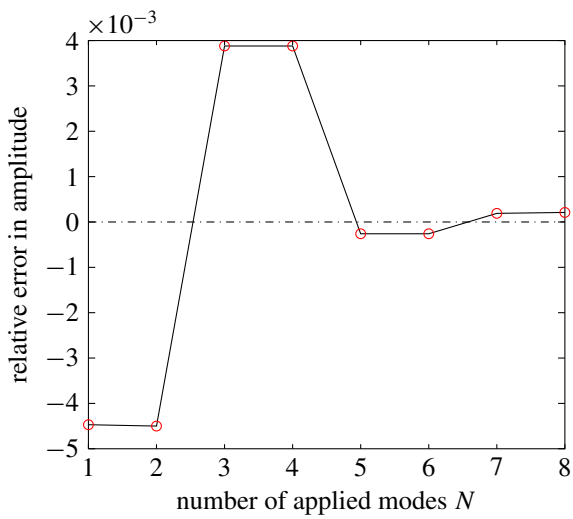

Figure 2. The relative error of numerical results for postbuckling amplitude as a function of the truncated mode number N for $\mu = 0$, $f_I = 0$, $\alpha = 800$, and $p = 10\pi^2$.

5. Results and discussion

This section examines the nonlinear behavior of the CCMW employing the nonlinear model developed in Section 2. More specifically, the postbuckling amplitudes of the microwire are examined in Section 5.1, for different values of α and f_I. The effect of initial conditions on the postbuckling configurations (amplitude and shape) of the microwire is analyzed in Section 5.2. The influence of magnetic field parameter on the postbuckling configurations of the microwire is discussed in Section 5.3. Section 5.4 evaluates the effect of material length scale parameter on the stability and postbuckling amplitudes of the microwire. In Section 5.5, the effect of axial compressive load on the postbuckling configuration is studied.

5.1. ***Postbuckling amplitudes of the microwire for various α and f_I.*** The microwire's stability and postbuckling amplitude are examined by setting $\mu = 0.1$ and $p = 0$, and varying the value of α. To observe the stability evolution of the microwire, the dimensionless magnetic force f_I is successively increased.

Figure 3 shows the buckling responses of the microwire through plots of the transverse amplitudes as a function of f_I, for clamped-clamped or pinned-pinned boundary conditions. The results are obtained for a microwire with $\alpha = 800$, 1200, 1600, or 2000. In Figure 3, the transverse amplitudes of the microwire are denoted as $\max(\sqrt{\bar{v}(\xi,\tau)^2 + \bar{w}(\xi,\tau)^2})$. From this figure, one may find that the buckling instability of a clamped-clamped microwire occurs at $f_{Ic} \approx 0.0192$, 0.0104, 0.0068, and 0.0048 for four different values of α ($\alpha = 800$, 1200, 1600, and 2000), respectively. For a pinned-pinned microwire, the buckling instability occurs at $f_{Ic} \approx 0.0069$, 0.0038, 0.0024, and 0.0018 for $\alpha = 800$, 1200, 1600, and 2000, respectively. Since f_{Ic} represents the onset value of dimensionless magnetic force for buckling instability, it is termed as the critical magnetic force. Thus, by changing the value of α and maintaining other system parameters unchanged, the slenderness ratio parameter α is found to have significant effect on the critical magnetic force and hence the postbuckling amplitudes of the microwire. The evolution of postbuckling amplitudes as a function of α is in accord with one's common experience. Based on further calculations, it is found that at the onset of buckling instability, we have $\alpha^{3/2} f_{Ic} \approx 433.7$ for clamped-clamped ends and $\alpha^{3/2} f_{Ic} \approx 157.1$ for pinned-pinned ends. For a given set of boundary conditions, therefore, the combined parameter $\alpha^{3/2} f_I$ may be viewed as an essential index for examining the stability of CCMW acted upon by a longitudinal magnetic field. In the following discussion, we define $\alpha^{3/2} f_I$ as a new magnetic field parameter.

5.2. ***Postbuckling configurations for various*** **initial conditions.** The results shown in Figure 3 were concerned with the transverse amplitudes of the microwire. Some calculations for the postbuckling shapes of the microwire are further conducted here. In our numerical calculations, it is noted that the initial conditions can significantly affect the final postbuckling shapes of the microwire. This trend may be the most interesting finding in this work. Some typical results are plotted in Figure 4 and Figure 5, where the dimensionless magnetic field parameter $\alpha^{3/2} f_I$ remains unchanged while the value of α is varied. In Figure 4, the initial conditions for calculations were chosen as

$$\dot{\boldsymbol{q}}_v(0) = \dot{\boldsymbol{q}}_w(0) = \{0, 0, 0, 0, 0\}, \quad \boldsymbol{q}_v(0) = \boldsymbol{q}_w(0) = \{a, 0, 0, 0, 0\}, \tag{38}$$

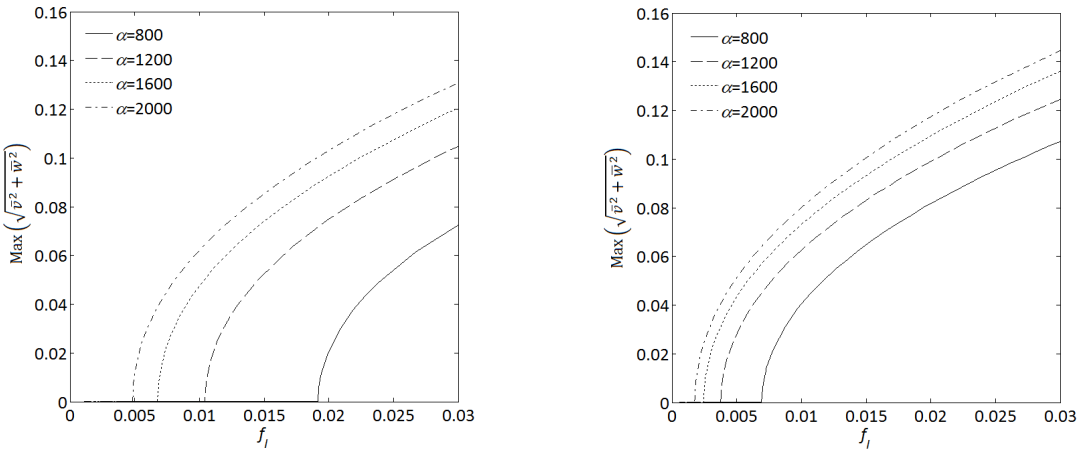

Figure 3. The maximum transverse amplitudes of the microwire as a function of the dimensionless magnetic force f_I, for $\mu = 0.1$, $p = 0$, and various values of α: for clamped-clamped boundary conditions (left), and for pinned-pinned boundary conditions (right).

where a is a given constant and is fixed to be 0.001 in our calculations. In Figure 5, however, another set of initial conditions were used:

$$\dot{\boldsymbol{q}}_v(0) = \dot{\boldsymbol{q}}_w(0) = \{0, 0, 0, 0, 0\}, \quad \boldsymbol{q}_v(0) = \{a, 0, 0, 0, 0\}, \quad \boldsymbol{q}_w(0) = \{0, a, 0, 0, 0\}. \tag{39}$$

As shown by the results of Figure 4 and Figure 5, for a given set of system parameters, the buckling shapes in the x-o-y and x-o-z planes are different from each other. Interestingly, the postbuckling shapes depend on the combined parameter $\alpha^{3/2} f_I$ and the buckling amplitudes are affected by the slenderness ratio parameter α. Moreover, the postbuckling configurations shown in Figure 4 (left column) (or Figure 4, right column) contain both first-mode and second-mode components of a beam with clamped-clamped (or pinned-pinned) boundary conditions. As shown by the results of Figure 5, however, the postbuckling shapes for v in x-o-y plane and w in x-o-z plane mainly contains the first-mode and second-mode components, respectively.

More extensive calculations have been done for several other possible types of initial conditions. The results are presented in Figure 6 for clamped-clamped boundary conditions and in Figure 7 for pinned-pinned boundary conditions. From the results of Figure 6 and Figure 7, it is observed that the postbuckling shapes of the microwire are strongly dependent on the initial conditions used. For a set of given initial conditions, the buckling shape for v in the x-o-y plane may mainly contain the first-mode component of a clamped-clamped beam. For other initial conditions, however, it may be mainly associated with the second-mode component. To the authors' knowledge, this strong dependence of postbuckling shapes on the initial conditions is a relatively new finding for CCNWs and has not been reported previously.

An alternative, perhaps easier-to-understand form of the results of Figure 6 and Figure 7, is represented in a cylindrical coordinate, as shown in Figure 8 and Figure 9. In these two figures, the radius r and angle θ, respectively, denote the minimum distance from the deformed microwire to the x-axis and the minimum clockwise rotation angle from vector $\{v\,\boldsymbol{e}_y, w\,\boldsymbol{e}_z\}$ to the unit vector $\boldsymbol{e}_y$. From Figure 8

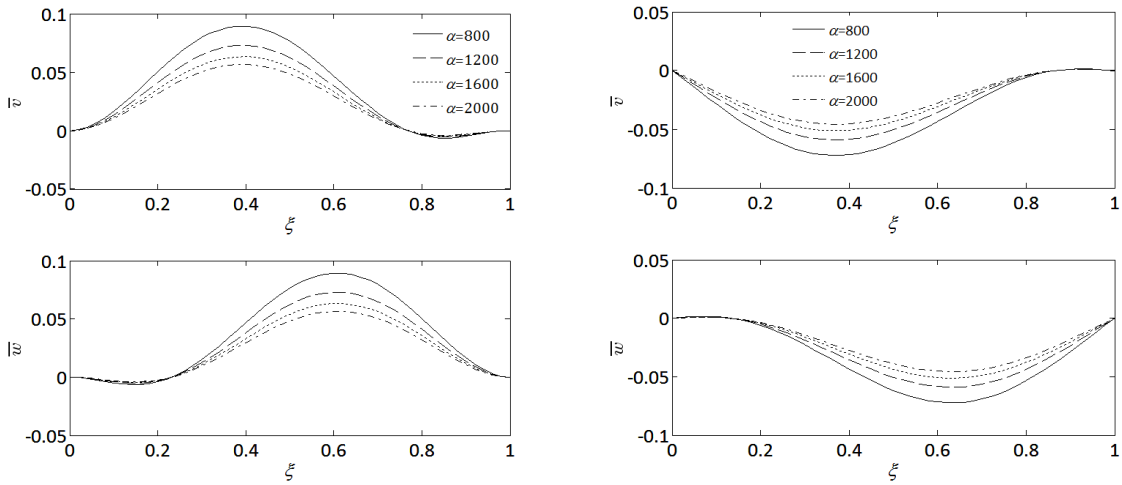

Figure 4. The postbuckling shapes of the microwire in the x-o-y and x-o-z planes for $\mu = 0.1$, $p = 0$, and various values of α, for: clamped-clamped boundary conditions with $\alpha^{3/2} f_I = 1000$ (left column), and pinned-pinned boundary conditions with $\alpha^{3/2} f_I = 500$; the initial conditions of (38) were chosen for all calculations (right column).

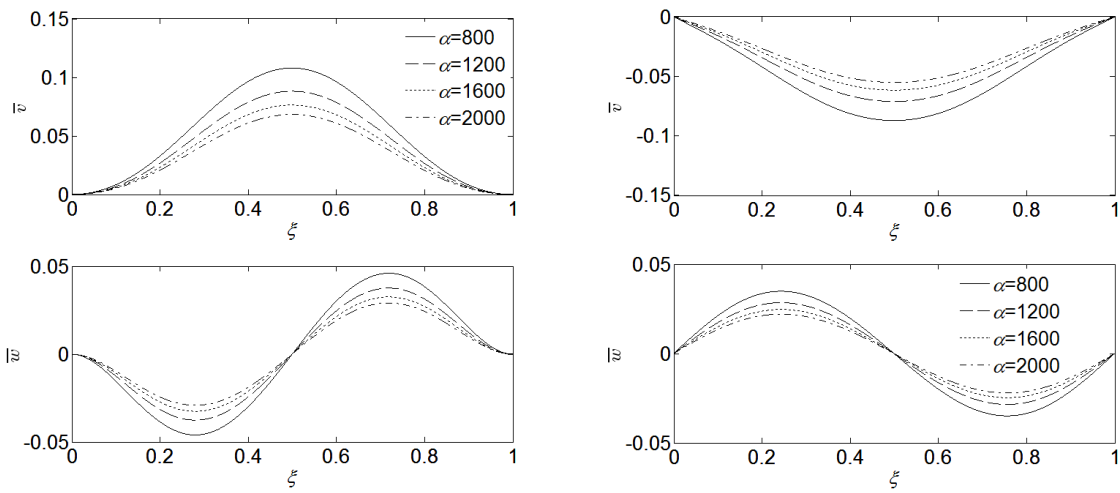

Figure 5. The postbuckling shapes of the microwire in the x-o-y and x-o-z planes for $\mu = 0.1$, $p = 0$, and various values of α, for: clamped-clamped boundary conditions with $\alpha^{3/2} f_I = 1000$ (left column), and pinned-pinned boundary conditions with $\alpha^{3/2} f_I = 500$; the initial conditions of (39) were chosen for all calculations (right column).

and Figure 9, one can observe two obvious but important features. First, the dimensionless radius r for a fixed ξ is identical for various different initial conditions, for either clamped-clamped or pinned-pinned boundary conditions. This implies that initial conditions have no effect on the "overall" nonplanar amplitudes of the CCMW. However, initial conditions can affect the spatial shapes of the microwire, as

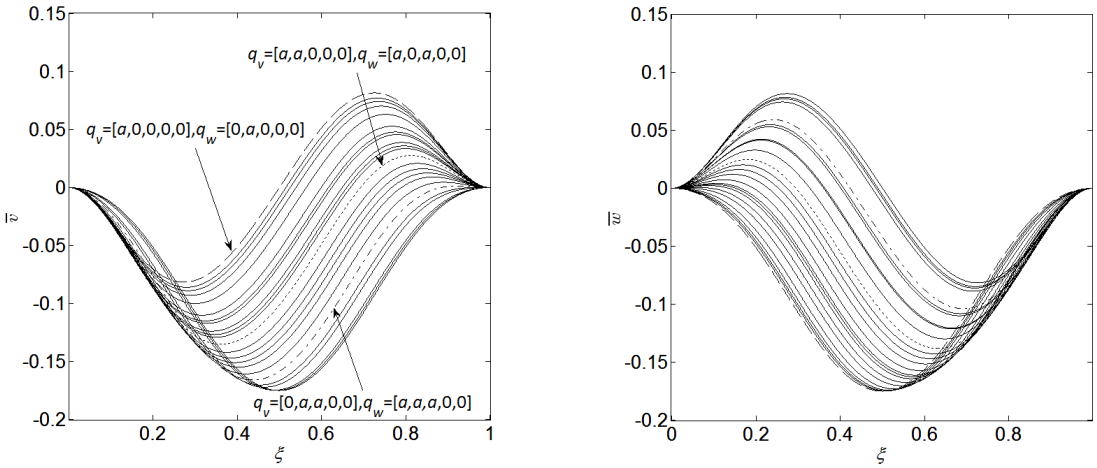

Figure 6. The postbuckling shapes of the microwire with clamped-clamped ends for different initial conditions: $\mu = 0.1$, $p = 0$, $\alpha^{3/2} f_I = 2000$, and $\alpha = 800$.

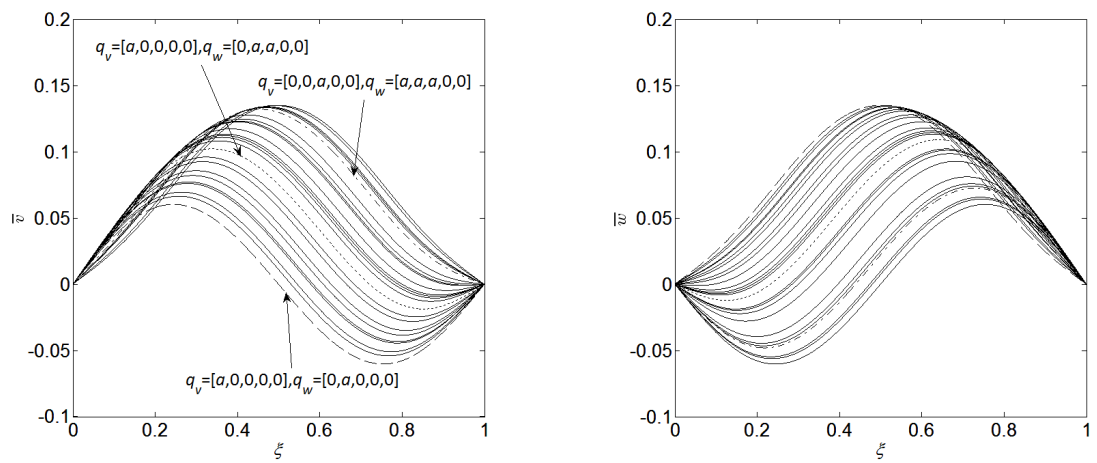

Figure 7. The postbuckling shapes of the microwire with pinned-pinned ends for different initial conditions: $\mu = 0.1$, $p = 0$, $\alpha^{3/2} f_I = 1000$, and $\alpha = 800$.

may be observed in Figure 8, right, and Figure 9, right. Second, the total relative rotation angles of clamped-clamped microwire and pinned-pinned microwire are 150 and 120 degrees respectively, which are independent of initial conditions.

To explain the strong dependence of postbuckling shapes on initial conditions, let us analyze the eigenvectors of the stiffness matrix $[\boldsymbol{K}]$ in (8). For a given set of system parameters, extensive calculations showed that the dimensionless axial elongation of the microwire's centerline do not change for various initial conditions. This means that the stiffness matrix $[\boldsymbol{K}]$ does not change. Putting the value of

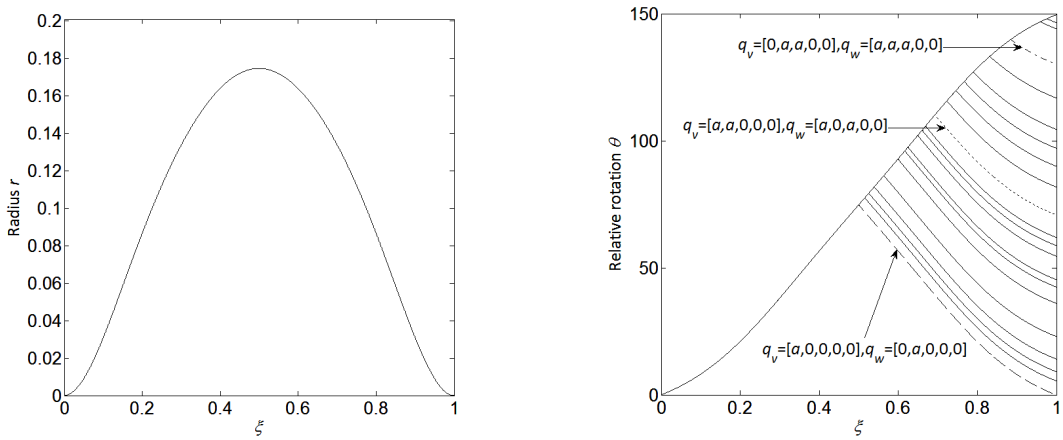

Figure 8. The postbuckling configurations of a clamped-clamped microwire shown in a cylindrical coordinate system for different initial conditions and $\mu = 0.1$, $p = 0$, $\alpha^{3/2} f_I = 2000$, and $\alpha = 800$.

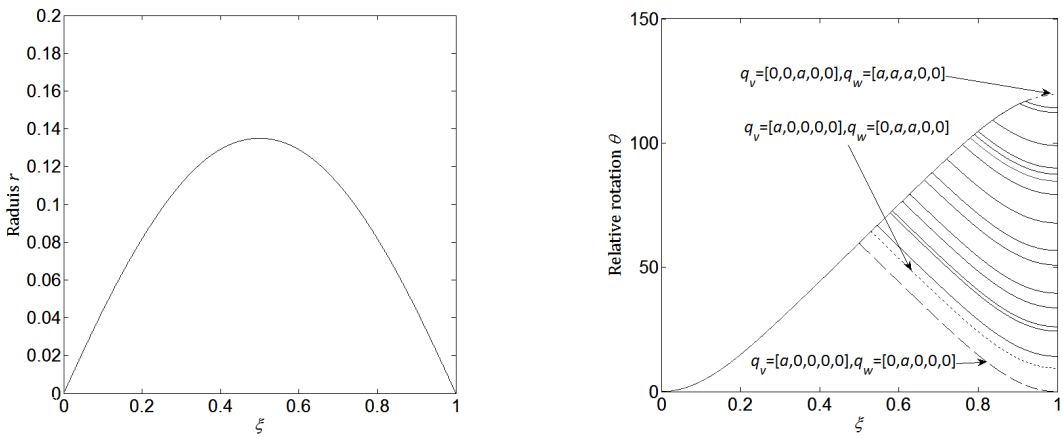

Figure 9. The postbuckling configurations of a pinned-pinned microwire shown in a cylindrical coordinate system, for different initial conditions and $\mu = 0.1$, $p = 0$, $\alpha^{3/2} f_I = 1000$, and $\alpha = 800$.

dimensionless axial elongation of the centerline into the stiffness matrix $[\boldsymbol{K}]$, one has

$$\begin{bmatrix} \boldsymbol{K}^{vv} & \boldsymbol{K}^{vw} \\ \boldsymbol{K}^{wv} & \boldsymbol{K}^{ww} \end{bmatrix} \begin{Bmatrix} \boldsymbol{q}_v \\ \boldsymbol{q}_w \end{Bmatrix} = 0. \tag{40}$$

It is assumed that a particular nontrivial solution of (40) may be expressed as

$$\begin{Bmatrix} \boldsymbol{q}_v \\ \boldsymbol{q}_w \end{Bmatrix} = \begin{Bmatrix} \boldsymbol{X}_1 \\ \boldsymbol{X}_2 \end{Bmatrix}. \tag{41}$$

Bearing in mind the expression of (29), one has

$$\boldsymbol{K}^{vv} = \boldsymbol{K}^{ww}, \quad \boldsymbol{K}^{vw} = -\boldsymbol{K}^{wv}. \tag{42}$$

It is noted that, therefore, another particular solution satisfying (40) can be written as

$$\begin{Bmatrix} \boldsymbol{q}_v \\ \boldsymbol{q}_w \end{Bmatrix} = \begin{Bmatrix} \boldsymbol{X}_2 \\ -\boldsymbol{X}_1 \end{Bmatrix}. \tag{43}$$

Thus, it follows from (41) and (43) that there may exist infinite kinds of possible solutions to (28). This implies that infinite kinds of postbuckling shapes may occur, mainly determined by the chosen initial conditions. Indeed, the feature of kaleidoscopic postbuckling shapes is due to the antisymmetry of the stiffness matrix $[\boldsymbol{K}]$. This new feature for nonplanar microwires has not been detected in previous studies of microwires under buckling in a single plane.

In fact, the initial displacement conditions may be viewed as an initial disturbance for the microwire. From this point of view, a set of initial velocity conditions may be also employed as an initial disturbance.

5.3. ***Effect of magnetic field parameter on the postbuckling configurations.*** The main results obtained, plotted in Figures 10–12, show that the magnetic field parameter may, sometimes, affect the postbuckling configurations of the microwire. In Figure 10 and Figure 11, four values of magnetic field parameter have been chosen for calculations for clamped-clamped or pinned-pinned boundary conditions. With initial conditions defined by (39), it is clear that the magnetic field parameter does not have visible effect on the postbuckling shape of the microwire. With initial conditions of (38), however, it is seen that the effect of magnetic field parameter on the postbuckling shape is obvious. For example, the results of Figure 10 (right) show that with increasing magnetic field parameter, the buckling shape of w in the x-o-z plane contains more and more second-mode components of a clamped-clamped beam. Similar trends may be found for pinned-pinned boundary conditions.

In addition, it is found that the buckling instability cannot appear in higher-order modes (e.g., the third mode), even if the magnetic field parameter becomes sufficiently large.

More extensive calculations have produced the results of Figure 12, where the initial conditions of (38) were utilized, for either clamped-clamped or pinned-pinned boundary conditions. In Figure 12 (left or right), twenty different values of magnetic field parameter were selected for calculations, thus producing twenty curves in each figure. Only the configurations of v have been plotted for clarity. It should be stated that the results of postbuckling amplitudes shown in Figure 12 have been normalized for the purpose of intuitive comparison. From Figure 12 (left and right), it is clearly seen that, with the increase of magnetic field parameter, the postbuckling configuration evolves from the first-mode shape to a hybrid shapes of both first and second modes.

Strictly speaking, the displacement v (or w) would contain contributions of all the modes according to the basic idea of the Galerkin's approach. However, the contributions of higher-order modes are not pronounced, as demonstrated in Figure 13, in which the proportions of the lowest four modes for determining the displacement of v have been quantitatively shown. It is observed that the microwire's displacement is mainly associated with the first and second modes. With the increase of magnetic field parameter, the first-mode contribution becomes smaller while the second-mode contribution becomes larger.

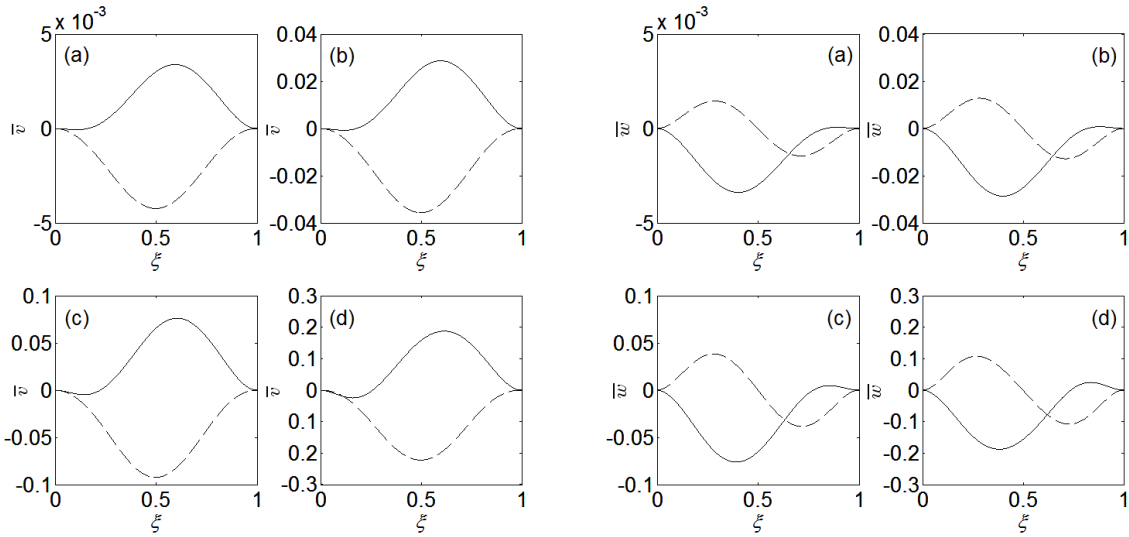

Figure 10. The evolution of postbuckling shapes of clamped-clamped microwires with increasing magnetic field parameter for $\mu = 0.1$, $p = 0$, and $\alpha = 800$: (a) $\alpha^{3/2} f_I = 435$, (b) $\alpha^{3/2} f_I = 495$, (c) $\alpha^{3/2} f_I = 900$, (d) $\alpha^{3/2} f_I = 3300$. Solid lines indicate results where initial conditions were from (38), and dashed lines indicate results where initial conditions were from (39).

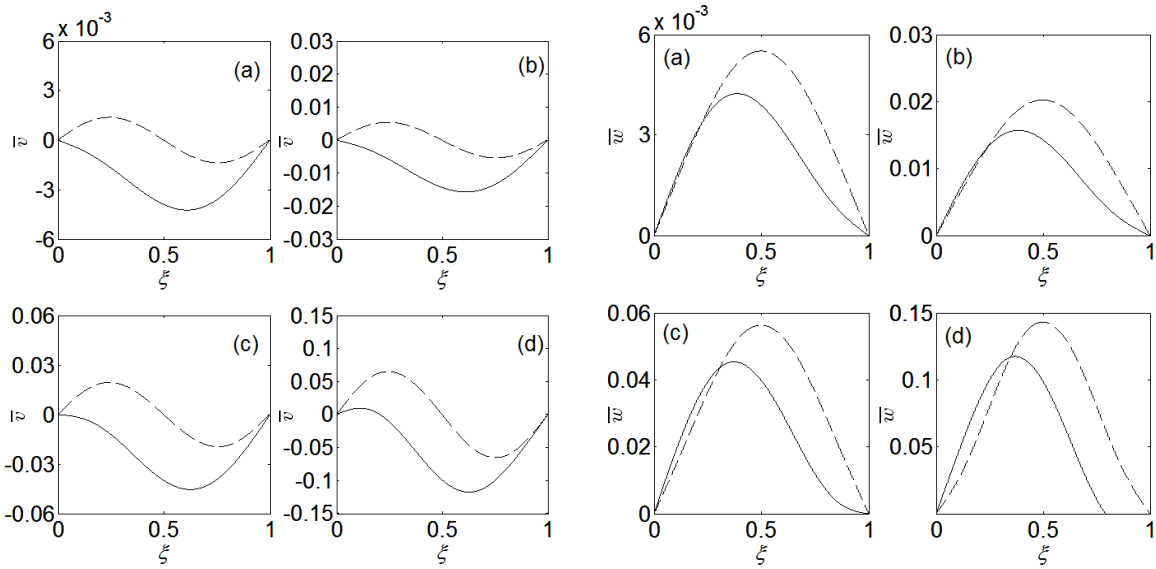

Figure 11. The evolution of postbuckling shapes of pinned-pinned microwires with increasing magnetic field parameter for $\mu = 0.1$, $p = 0$, and $\alpha = 800$: (a) $\alpha^{3/2} f_I = 158$, (b) $\alpha^{3/2} f_I = 176$, (c) $\alpha^{3/2} f_I = 308$, (d) $\alpha^{3/2} f_I = 1155$; Solid lines indicate results where initial conditions were from (38), and dashed lines indicate results where initial conditions were from (39).

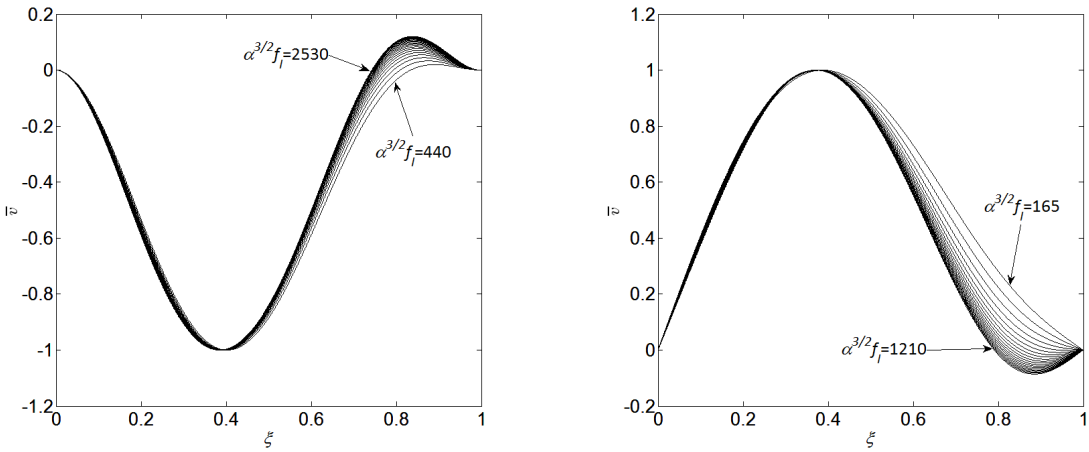

Figure 12. The effect of magnetic field parameter on the postbuckling shapes of v for $\mu = 0.1$, $p = 0$, and $\alpha = 800$: clamped-clamped boundary conditions (left) and pinned-pinned boundary conditions (right).

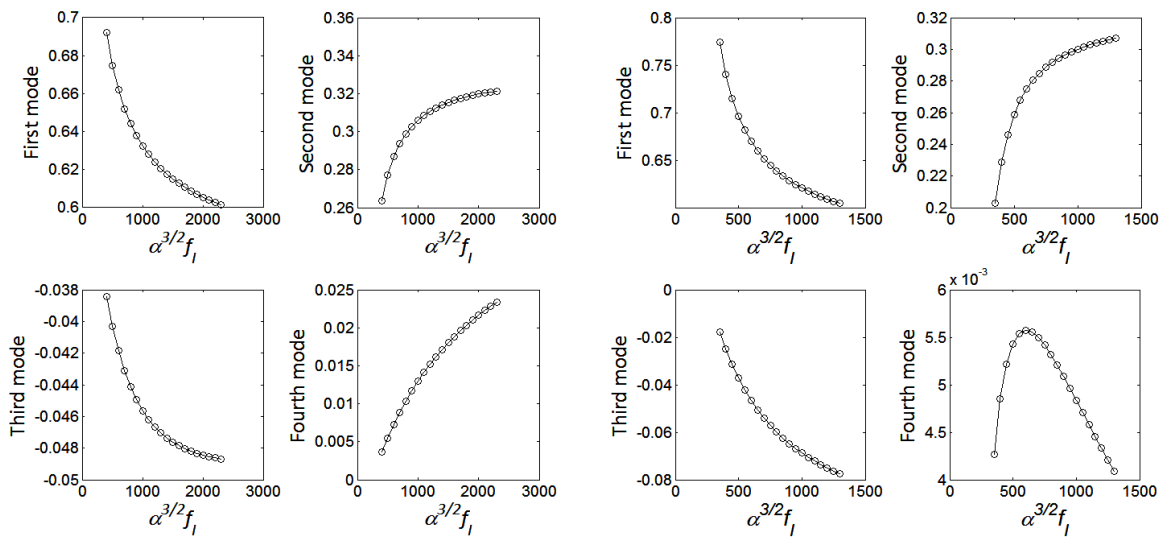

Figure 13. The proportions of the lowest four modes for various magnetic field parameters and $\mu = 0.1$, $p = 0$, and $\alpha = 800$: clamped-clamped boundary conditions (left) and pinned-pinned boundary conditions (right).

5.4. ***Effect of material length scale parameter on the stability boundaries.*** The stability problem of a slender beam has been investigated by many researchers. In particular, the exact solution of postbuckling configurations of beams has been obtained by Nayfeh and his coworkers [Nayfeh and Emam 2008]. In this section, the stability boundaries of the CCMW under both axial compression and magnetic force are studied, for various values of dimensionless material length scale parameter μ, to show the effect of μ on the buckling behaviors of the microwire. Typical results with $\alpha = 800$ are shown in Figure 14

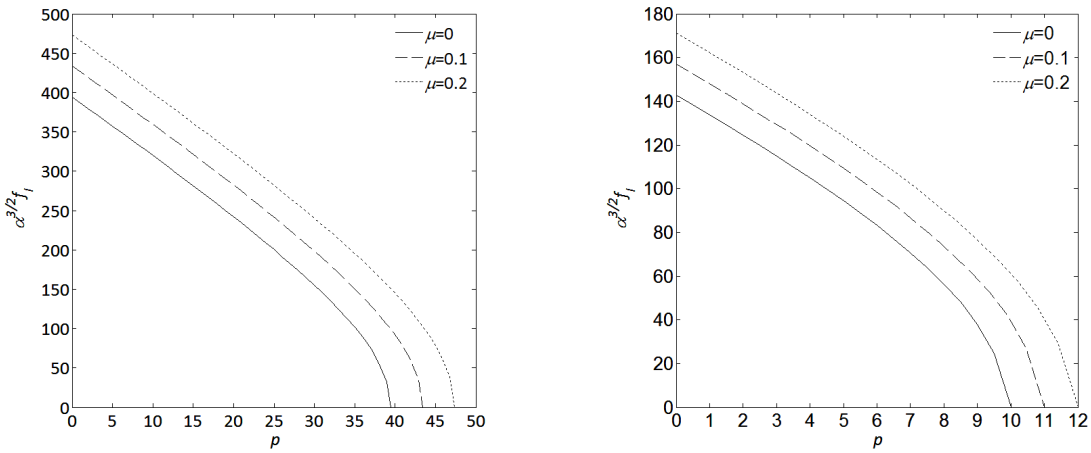

Figure 14. The stability boundaries for $\alpha = 800$ and $\mu = 0$, 0.1, and 0.2 for clamped-clamped and (left) and pinned-pinned boundary conditions (right).

and Figure 15, for both clamped-clamped and pinned-pinned boundary conditions. The dimensionless material length scale parameter is chosen to be $\mu = 0$, 0.1, and 0.2 for calculations.

The results given in Figure 14 show the stability boundaries for $\mu = 0$, 0.1, and 0.2. From Figure 14, it is noted that the critical magnetic field parameter is $\alpha^{3/2} f_{Ic} \approx 394.3$ for $p = 0$ and $\mu = 0$, which is in accordance with the linear result of Wang et al. [2015] for microwires with clamped-clamped ends. It is obviously seen that the material length scale parameter can stabilize the microwire system while both the magnetic field parameter and axial compression would destabilize the microwire. When the magnetic field parameter and axial compression are small and locate below the stability boundary, the microwire is stable. If, however, the magnetic field parameter and axial compression are large and locate beyond the stability boundary, the microwire is buckled. Utilizing the critical buckling curves shown in Figure 14, an expected critical value of magnetic field parameter may be achieved by choosing a suitable compressive load as a trigger of automatic devices.

Based on the nonlinear governing equations of (26), the maximum amplitudes of lateral displacements ($\max[\sqrt{\bar{v}(\xi,\tau)^2 + \bar{w}(\xi,\tau)^2}\,]$) are plotted in Figure 15. It is observed that the material length scale can decrease the buckling amplitudes of the microwire, again, indicating that the material length scale parameter plays a stabilizing effect on the microwire system.

5.5. ***Effect of axial compression on the postbuckling configurations.*** The effect of axial compression on the postbuckling configurations of the microwire can be seen in Figure 16, where the parameters were chosen as $\mu = 0.1$, $\alpha^{3/2} f_I = 1000$, and $\alpha = 800$. The initial conditions defined by (38) were used for calculations. An interesting feature of Figure 16 is that the axial compression does not affect the postbuckling shapes at all, although it does affect the postbuckling amplitudes of the microwire. This implies that the main role of an axial compression is to promote the occurrence of buckling instability and change the postbuckling amplitude of the microwire. Thus, even if the axial compression is sufficiently large, the postbuckling configuration (shape) is still dominated by the first-order mode or the second-order mode. In fact, higher modes can only slightly affect the postbuckling configuration of the microwire.

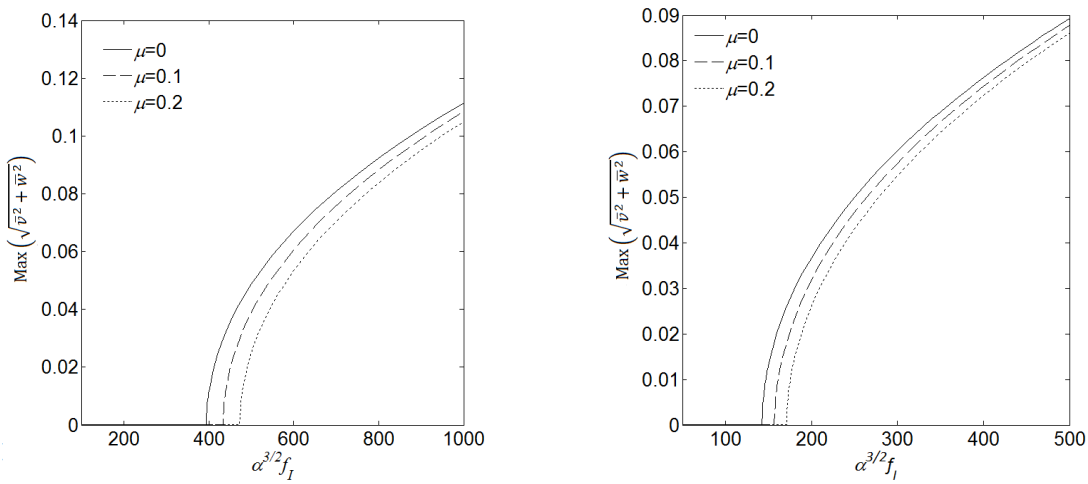

Figure 15. The maximum amplitude of lateral displacements as a function of the dimensionless magnetic field parameter for $\alpha = 800$, $p = 0$ and three different values of μ for clamped-clamped and (left) and pinned-pinned boundary conditions (right).

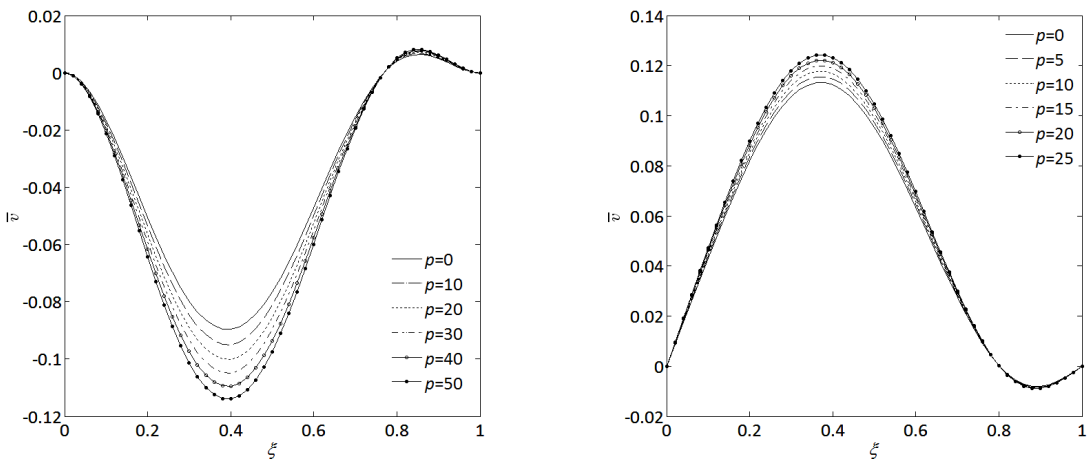

Figure 16. The evolution of postbuckling configurations of the microwire with increasing axial compression for $\mu = 0.1$, $\alpha = 800$, and $\alpha^{3/2} f_I = 1000$: with clamped-clamped boundary conditions (left), and with pinned-pinned boundary conditions; all results were obtained using initial conditions of (38) (right).

Before leaving Section 5, it should be mentioned that the stability and postbuckling response of the microwire were not analyzed from the point of view of energy, although the governing equations were derived from Hamilton's principle. In the above analysis, the postbuckling responses and critical loads were evaluated by numerically solving (26). The connection with energy of the system in the pre- and post-buckling responses may be another interesting topic for the system of current-carrying microwires. This needs more extensive analysis in the future.

6. Conclusions

This paper studies the stability and nonplanar postbuckling of a current-carrying microwire subjected to a longitudinal magnetic field, by taking into account the geometric nonlinearities caused by the axial elongation of the microwire's centerline. Based on the Euler–Bernoulli beam assumptions, the modified couple stress theory and Hamilton's principle, the dimensionless version of nonplanar nonlinear equations of the microwire is derived. Using the Galerkin's approach and a fourth-order Runge–Kutta method, numerical results for both clamped-clamped and pinned-pinned boundary conditions are obtained. The effects of several dimensionless parameters associated with slenderness ratio, magnetic field, compressive load, and material length scale on the nonplanar buckling and postbuckling configurations are analyzed. Among others, some major conclusions are summarized as follows:

The slenderness ratio parameter α has an obvious effect on the stability and the postbuckling amplitude of the microwire. The most interesting result obtained is that the nonplanar postbuckling shapes of the microwire under a longitudinal magnetic field may change when the initial conditions were varied, indicating that the nontrivial equilibria are sensitive to the initial conditions used for calculations. The dependence of postbuckling shapes on initial conditions makes it difficult to accurately determine the final postbuckling configurations of the microwires in practice. It is also expected that such high sensitivity of postbuckling configurations to initial conditions can be validated experimentally in the future. If such sensitivity is physically true, then how to minimize or control such a sensitivity is another interesting topic. In addition, one may also envision that some other methods such as a stochastic approach, or perhaps a statistical method can help understand such a sensitivity further.

The influence of magnetic field parameter on the postbuckling shapes is found to be remarkable in many cases. With the increase of magnetic field parameter, the postbuckling configurations are mostly associated with the first- and second-mode components, and the proportion of the second-mode component becomes larger while the proportion of the first-mode component decreases. In all cases, the proportion of higher-order modes (e.g., third or fourth modes) is low and may be neglected.

The effect of material length scale parameter on the stability and postbuckling amplitude of the microwire may be foreseen using one's experience. With the increase of dimensionless material length scale parameter, the microwire becomes more stable. For a buckled microwire, the postbuckling amplitude would decrease with increasing material length scale parameter.

Finally, it is found that the axial compressive load has an obvious effect on the postbuckling amplitude while it does not affect the postbuckling shape of the microwire. Moreover, the presence of an axial compression may reduce the threshold value of the magnetic field parameter for buckling instability.

Acknowledgment

This work is supported by the National Natural Science Foundation of China (No. 11572133).

References

[Arani et al. 2015] A. G. Arani, P. Dashti, S. Amir, and M. Yousefi, "Nonlinear vibration of coupled nano- and microstructures conveying fluid based on Timoshenko beam model under two-dimensional magnetic field", *Acta Mech.* **226**:8 (2015), 2729–2760.

[Atashbar and Singamaneni 2005] M. Z. Atashbar and S. Singamaneni, "Room temperature gas sensor based on metallic nanowires", *Sens. Actuator B Chem.* **111-112** (2005), 13–21.

[Chang 2016] T.-P. Chang, "Nonlinear free vibration analysis of nanobeams under magnetic field based on nonlocal elasticity theory", *J. Vibroeng.* **18**:3 (2016), 1912–1919.

[Chang and Yeh 2014] T.-P. Chang and Q.-J. Yeh, "Nonlinear free vibration of nanobeams subjected to magnetic field based on nonlocal elasticity theory", in *International Conference of Scientific Computing '14*, edited by H. R. Arabnia et al., 2014.

[Dai et al. 2015] H. L. Dai, Y. K. Wang, and L. Wang, "Nonlinear dynamics of cantilevered microbeams based on modified couple stress theory", *Int. J. Eng. Sci.* **94** (2015), 103–112.

[Dehrouyeh-Semnani et al. 2015] A. M. Dehrouyeh-Semnani, M. Dehrouyeh, M. Torabi-Kafshgari, and M. Nikkhah-Bahrami, "An investigation into size-dependent vibration damping characteristics of functionally graded viscoelastically damped sandwich microbeams", *Int. J. Eng. Sci.* **96** (2015), 68–85.

[Ebrahimi and Barati 2016] F. Ebrahimi and M. R. Barati, "Dynamic modeling of a thermo–piezo-electrically actuated nanosize beam subjected to a magnetic field", *Appl. Phys. A Mater. Sci. Process.* **122** (2016), 451.

[Ebrahimi and Barati 2017a] F. Ebrahimi and M. R. Barati, "Flexural wave propagation analysis of embedded S-FGM nanobeams under longitudinal magnetic field based on nonlocal strain gradient theory", *AJSE* **42**:5 (2017), 1715–1726.

[Ebrahimi and Barati 2017b] F. Ebrahimi and M. R. Barati, "Flexural wave propagation analysis of embedded S-FGM nanobeams under longitudinal magnetic field based on nonlocal strain gradient theory", *AJSE* **42**:5 (2017), 1715–1726.

[Fleck et al. 1994] N. A. Fleck, G. M. Muller, M. F. Ashby, and J. W. Hutchinson, "Strain gradient plasticity: theory and experiment", *Acta Metall. Mater.* **24**:2 (1994), 475–487.

[He and Lilley 2008] J. He and C. M. Lilley, "Surface stress effect on bending resonance of nanowires with different boundary conditions", *Appl. Phys. Lett.* **93** (2008), 263108.

[Kahrobaiyan et al. 2011] M. H. Kahrobaiyan, M. Asghari, M. Rahaeifard, and M. T. Ahmadian, "A nonlinear strain gradient beam formulation", *Int. J. Eng. Sci.* **49**:11 (2011), 1256–1267.

[Kiani 2014a] K. Kiani, "Forced vibrations of a current-carrying nanowire in a longitudinal magnetic field accounting for both surface energy and size effects", *Physica E* **63** (2014), 27–35.

[Kiani 2014b] K. Kiani, "Surface effect on free transverse vibrations and dynamic instability of current-carrying nanowires in the presence of a longitudinal magnetic field", *Phys. Lett. A* **378**:26-27 (2014), 1834–1840.

[Kiani 2014c] K. Kiani, "Vibration and instability of a single-walled carbon nanotube in a three-dimensional magnetic field", *J. Phys. Chem. Solids* **75**:1 (2014), 15–22.

[Kiani 2015a] K. Kiani, "Axial buckling analysis of a slender current-carrying nanowire acted upon by a magnetic field using the surface energy approach", *J. Phys. D Appl. Phys.* **48**:24 (2015), 245302.

[Kiani 2015b] K. Kiani, "Vibrations and instability of pretensioned current-carrying nanowires acted upon by a suddenly applied three-dimensional magnetic field", *Mater. Chem. Phys* **162** (2015), 531–541.

[Kiani 2016] K. Kiani, "Column buckling of doubly parallel slender nanowires carrying electric current acted upon by a magnetic field", *J. Phys. Chem. Solids* **95** (2016), 89–97.

[Lee et al. 2008] J.-Y. Lee, S. T. Connor, Y. Cui, and P. Peumans, "Solution-processed metal nanowire mesh transparent electrodes", *Nano Lett.* **8**:2 (2008), 689–692.

[Lee et al. 2013] J.-H. Lee, H.-S. Shin, Y.-J. Noh, S.-I. Na, and H.-K. Kim, "Brush painting of transparent PEDOT/Ag nanowire/PEDOT multilayer electrodes for flexible organic solar cells", *Sol. Energy Mater Sol. Cells* **114** (2013), 15–23.

[Li et al. 2007] Q. Li, S.-M. Koo, M. D. Edelstein, J. S. Suehle, and C. A. Richter, "Silicon nanowire electromechanical switches for logic device application", *Nanotechnology* **18**:31 (2007), 315202.

[Luo et al. 2006] L. Luo, Y. Zhang, S. S. Mao, and L. Lin, "Fabrication and characterization of ZnO nanowires based UV photodiodes", *Sens. Actuators A Phys.* **127**:2 (2006), 201–206.

[McFarland and Colton 2005] A. W. McFarland and J. S. Colton, "Role of material microstructure in plate stiffness with relevance to microcantilever sensors", *J. Micromech. Microeng.* **15**:5 (2005), 1060.

[Mindlin and Tiersten 1962] R. D. Mindlin and H. F. Tiersten, "Effects of couple-stresses in linear elasticity", *Arch. Ration. Mech. Anal.* **11**:1 (1962), 415–448.

[Mohammadabadi et al. 2015] M. Mohammadabadi, A. R. Daneshmehr, and M. Homayounfard, "Size-dependent thermal buckling analysis of micro composite laminated beams using modified couple stress theory", *Int. J. Eng. Sci.* **92** (2015), 47–62.

[Mojahedi and Rahaeifard 2016] M. Mojahedi and M. Rahaeifard, "A size-dependent model for coupled 3D deformations of nonlinear microbridges", *Int. J. Eng. Sci.* **100** (2016), 171–182.

[Narendar et al. 2012] S. Narendar, S. S. Gupta, and S. Gopalakrishnan, "Wave propagation in single-walled carbon nanotube under longitudinal magnetic field using nonlocal Euler–Bernoulli beam theory", *Appl. Math. Model.* **36**:9 (2012), 4529–4538.

[Nayfeh and Emam 2008] A. H. Nayfeh and S. A. Emam, "Exact solution and stability of postbuckling configurations of beams", *Nonlinear Dyn.* **54**:4 (2008), 395–408.

[Pauzauskie and Yang 2006] P. J. Pauzauskie and P. Yang, "Nanowire photonics", *Mater. Today* **9**:10 (2006), 36–45.

[Singh 2009] M. R. Singh, "Photonic transistors made from metallic photonic quantum wires", *Microelectron. J.* **40** (2009), 749–752.

[Stölken and Evans 1998] J. S. Stölken and A. G. Evans, "A microbend test method for measuring the plasticity length scale", *Acta Mater.* **46**:1 (1998), 5109–5115.

[Sun et al. 2017] X.-P. Sun, Y.-Z. Hong, H.-L. Dai, and L. Wang, "Nonlinear frequency analysis of buckled nanobeams in the presence of longitudinal magnetic field", *Acta Mech. Solida Sin.* **30**:5 (2017), 465–473.

[Tao et al. 2010] R.-H. Tao, J.-M. Wu, H.-X. Xue, X.-M. Song, X. Pan, X.-Q. Fang, X.-D. Fang, and S.-Y. Dai, "A novel approach to titania nanowire arrays as photoanodes of back-illuminated dye-sensitized solar cells", *J. Power Sources* **195**:9 (2010), 2989–2995.

[Tsiatas 2009] G. C. Tsiatas, "A new Kirchhoff plate model based on a modified couple stress theory", *Int. J. Solids Struct.* **46**:13 (2009), 2757–2764.

[Wang 2009] L. Wang, "Vibration and instability analysis of tubular nano- and micro-beams conveying fluid using nonlocal elastic theory", *Physica E* **41**:10 (2009), 1835–1840.

[Wang et al. 2006] C. M. Wang, Y. Y. Zhang, S. S. Ramesh, and S. Kitipornchai, "Buckling analysis of micro- and nano-rods/tubes based on nonlocal Timoshenko beam theory", *J. Phys. D Appl. Phys.* **39**:17 (2006), 3904.

[Wang et al. 2015] L. Wang, W.-B. Liu, and H.-L. Dai, "Dynamics and instability of current-carrying microbeams in a longitudinal magnetic field", *Physica E* **66** (2015), 87–92.

[Wang et al. 2016] L. Wang, Y. Hong, H. Dai, and Q. Ni, "Natural frequency and stability tuning of cantilevered CNTs conveying fluid in magnetic field", *Acta Mech. Solida Sin.* **29**:6 (2016), 567–576.

[Yang et al. 2002] F. Yang, A. C. M. Chong, D. C. C. Lam, and P. Tong, "Couple stress based strain gradient theory for elasticity", *Int. J. Solids Struct.* **39**:10 (2002), 2731–2743.

Received 22 Feb 2018. Revised 24 Jul 2018. Accepted 30 Jul 2018.

YUANZHUO HONG: hyzlink@qq.com
Department of Mechanics, Huazhong University of Science and Technology, Wuhan, China

and

Hubei Key Laboratory for Engineering Structural Analysis and Safety Assessment, Wuhan, China

LIN WANG: wanglindds@hust.edu.cn
Department of Mechanics, Huazhong University of Science and Technology, Wuhan, China

and

Hubei Key Laboratory for Engineering Structural Analysis and Safety Assessment, Wuhan, China

HU-LIANG DAI: daihulianglx@hust.edu.cn
Department of Mechanics, Huazhong University of Science and Technology, Wuhan, China

and

Hubei Key Laboratory for Engineering Structural Analysis and Safety Assessment, Wuhan, China

JOURNAL OF MECHANICS OF MATERIALS AND STRUCTURES

msp.org/jomms

Founded by Charles R. Steele and Marie-Louise Steele

See msp.org/jomms for submission guidelines.

JoMMS (ISSN 1559-3959) at Mathematical Sciences Publishers, 798 Evans Hall #6840, c/o University of California, Berkeley, CA 94720-3840, is published in 10 issues a year. The subscription price for 2018 is US $615/year for the electronic version, and $775/year (+$60, if shipping outside the US) for print and electronic. Subscriptions, requests for back issues, and changes of address should be sent to MSP.

JoMMS peer-review and production is managed by EditFLOW® from Mathematical Sciences Publishers.

PUBLISHED BY

mathematical sciences publishers

nonprofit scientific publishing

http://msp.org/

Journal of Mechanics of Materials and Structures
Volume 13, No. 4 July 2018